Published in final edited form as:
Cancer Res. 2015 April 15; 75(8): 1675–1681. doi:10.1158/0008-5472.CAN-14-2852.

Ibrutinib Exerts Potent Antifibrotic and Antitumor Activities in Mouse Models of Pancreatic Adenocarcinoma

Daniel Massó-Vallés[1], **Toni Jauset**[1], **Erika Serrano**[1], **Nicole M. Sodir**[2], **Kim Pedersen**[1], **Nesrine I. Affara**[3], **Jonathan R. Whitfield**[1], **Marie-Eve Beaulieu**[1], **Gerard I. Evan**[2,3], **Laurence Elias**[4], **Joaquín Arribas**[1,5], **Laura Soucek**[1,5]

[1]Vall d'Hebron Institute of Oncology (VHIO), Edifici Mediterrània, Hospital Vall d'Hebron, Barcelona, Spain

[2]Department of Biochemistry, University of Cambridge, Cambridge, United Kingdom

[3]Department of Pathology, University of California, San Francisco, California

[4]Pharmacyclics Inc., Sunnyvale, California

[5]Institució Catalana de Recerca i Estudis Avançats (ICREA), Barcelona, Spain

Abstract

Pancreatic ductal adenocarcinoma (PDAC) is characterized by a dense stromal fibroinflammatory reaction that is a major obstacle to effective therapy. The desmoplastic stroma comprises many inflammatory cells, in particular mast cells as key components of the PDAC microenvironment, and such infiltration correlates with poor patient outcome. Indeed, it has been hypothesized that stromal ablation is critical to improve clinical response in patients with PDAC. Ibrutinib is a clinically approved Bruton's tyrosine kinase inhibitor that inhibits mast cells and tumorprogression in a mouse model of β-cell tumorigenesis. Here, we show that ibrutinib is highly effective at limiting the growth of PDAC in both transgenic mouse and patient-derived xenograft models of the disease. In these various experimental settings, ibrutinib effectively diminished fibrosis, extended survival, and improved the response to clinical standard-of-care therapy. Our

Corresponding Author: Laura Soucek, Vall d'Hebron Institute of Oncology (VHIO), Edifici Mediterrània, Hospital Vall d'Hebron, Psg. Vall d'Hebron 119, Barcelona 08035, Spain. Phone: 34-934894175; Fax: 34-934894015; lsoucek@vhio.net.

Disclosure of Potential Conflicts of Interest
L. Elias is the senior director of Pharmacyclics Inc., has ownership interest (including patents) in Pharmacyclics Inc. (Stockholder), and is a consultant/advisory board member for Pharmacyclics Consultant (Contractor). L. Soucek is a consultant/advisory board member for Pharmacyclics Inc. No potential conflicts of interest were disclosed by the other authors.

Authors' Contributions
Conception and design: D. Massó-Vallés, T. Jauset, N.M. Sodir, L. Elias, J. Arribas, L. Soucek
Development of methodology: D. Massó-Vallés, K. Pedersen, G. Evan, L. Soucek
Acquisition of data (provided animals, acquired and managed patients, provided facilities, etc.): D. Massó-Vallés, T. Jauset, E. Serrano, N.M. Sodir, Pedersen, N.I. Affara, L. Soucek
Analysis and interpretation of data (e.g., statistical analysis, biostatistics, computational analysis): D. Massó-Vallés, T. Jauset, E. Serrano, N.I. Affara, M.-E. Beaulieu, L. Elias, L. Soucek
Writing, review, and/or revision of the manuscript: D. Massó-Vallés, T. Jauset, J.R. Whitfield, L. Elias, J. Arribas, L. Soucek
Administrative, technical, or material support (i.e., reporting or organizing data, constructing databases): D. Massó-Vallés, E. Serrano, N.M. Sodir, G. Evan, L. Soucek
Study supervision: D. Massó-Vallés, J.R. Whitfield, L. Soucek

Europe PMC Funders Author Manuscripts

results offer a preclinical rationale to immediately evaluate the clinical efficacy of ibrutinib in patients with PDAC.

Introduction

Pancreatic cancer is the fourth most common cause of cancer death in the Western world and, although cancer mortality has in general been recently improving, it has a uniquely negative mortality trend in both sexes (1, 2). It is usually diagnosed at an advanced stage and characterized by poor prognosis. According to the American Cancer Society, the overall survival rates at 1 and 5 years are only 25% and 6%, respectively. The 5-year survival for localized disease is approximately 20%, and the median survival is 10 and 6 months for advanced and metastatic disease (which affects 80% of individuals), respectively (www.cancernetwork.com). Hence, there is an urgent need for new and effective therapies. Pancreatic adenocarcinoma is characterized by dense desmoplasia, composed of extracellular matrix, endothelial cells, immune cells, fibroblasts, and stellate cells. This epithelial and stromal compartment appears to enhance the aggressive nature of the disease and its resistance to therapy. Indeed, the dense stromal fibroinflammatory reaction results in decreased blood supply, poor drug delivery (3), and hypoxia (4). Hence, therapies targeting the stroma may be key to improving the clinical outcomes for patients with pancreatic cancer.

Analysis of human pancreatic ductal adenocarcinoma (PDAC) samples reported that mast cell infiltration correlated with higher tumor grade and worse survival (5), and high mast cell numbers at the intratumoral border correlated with the presence of lymphatic and microvascular invasion, as well as with lymph node metastasis (6). We have previously utilized a mouse model of pancreatic β-cell tumorigenesis to show that mast cells are required for angiogenesis and the macroscopic expansion and maintenance of tumors (7), thereby proposing mast cell targeting as a therapeutic strategy in such tumors. Since then, other groups have shown that this role for mast cells might be conserved in PDAC. For example, an influx of mast cells was observed in a mouse model of pancreatic cancer expressing high levels of $KRAS^{G12V}$ (8) and, importantly, pancreatic tumors orthotopically transplanted in mast cell-deficient mice grew more slowly than in control mice (8), conferring a survival advantage compared with tumors grown in mast cell proficient animals.

PCI-32765 (also known as ibrutinib) is a novel inhibitor of Bruton's tyrosine kinase (BTK) approved for the treatment of mantle cell lymphoma and chronic lymphocytic leukemia (CLL) patients who have received at least one previous therapy, and CLL patients with 17p deletion (9). It is known to be capable of inhibiting mast cell or basophil degranulation (10). Recently, we validated ibrutinib as a potent systemic mast cell blocker in our mouse model of insulinoma, triggering collapse of tumor vasculature and tumor regression (11). Hence, in the present study, we sought to investigate the potential therapeutic impact of ibrutinib in a preclinical model of PDAC.

Europe PMC Funders Author Manuscripts

Materials and Methods

IHC and collagen staining

For IHC analyses, tissue samples were fixed overnight in neutral pH–buffered formalin, embedded in paraffin, and sectioned (5 μm). Sections were then deparaffinized, rehydrated, and microwaved for 1 minute in 0.01 mol/L citrate buffer (pH 6.0) for antigen retrieval. Primary antibodies [rat monoclonal anti–CD11b (clone M1/70), eBioscience; rabbit polyclonal anti-CD11b, Novus Biologicals; rat monoclonal anti-F4/80 (clone CI:A3-1); rabbit monoclonal anti-Ki-67 (clone SP6), Neomarkers] were applied for 2 hours in blocking buffer (2.5% BSA, 5% goat serum, and 0.3% Triton X-100 in PBS), followed by Vectastain ABC kit and DAB reagents (Vector Laboratories). We identified mast cells by using 1% toluidine blue dissolved in ethanol. Picrosirius Red Stain Kit (Polysciences, Inc.) was used to stain for collagen types I and III according to manufacturer instructions. Images were obtained with an Axiovert S100 TV inverted fluorescence microscope (Zeiss) and Open Lab 3.5.1 software, with an Axiovert 100 inverted microscope (Zeiss) equipped with a Hamamatsu Orca digital camera or with an Olympus FSX100 microscope and FSX-BSW software.

Flow cytometry

Following resection, PDAC tumors isolated from PBS-perfused mice were immediately placed in ice-cold PBS, followed by manual mincing using scissors and a 20-minute enzymatic digestion with 1.25 mg/mL collagenase type IV (Roche), 0.1% trypsin inhibitor, and 50 U/mL DNase I (Roche) in serum-free DMEM (Life Technologies) at 37°C with continuous stirring. Single cell suspensions were then prepared by passing tissue through 70 μm nylon strainers (BD Biosciences). Cells were incubated for 30 minutes at 4°C with rat anti-mouse CD16/CD32 mAb (1:250, clone 2.4G2, BD Bioscience) in PBS, which also contained Live/Dead Aqua stain (1:250, Invitrogen) to differentiate between viable and dead cells. Cells were then incubated for 30 minutes in PBS containing 1.0% BSA (Sigma) and 2 mmol/L EDTA with 100 μL of fluorophore-conjugated anti-mouse antibodies (dilution; clone): PE-Cy7-CD45 (1:800; 30-F11), PerCp-Cy5.5-CD3e (1:400; 145-2C11), PerCp-Cy5.5-CD19 (1:200; 6D5), PerCp-Cy5.5-CD49b (1:400; DX5), Alexa 700-CD11b (1:400; M1/70), APC780-CD11c (1:200; N418), eFluor450-MHCII (1:800; M5/114.15.2), APC-Ly6C (1:800; HK1.4), PE-Ly6G (1:400; 1A8), and PE-Cy5-F4/80 (1:400; BM8; eBioscience or Biolegend). Cells were then washed once in PBS containing 1.0% BSA (Sigma) and 2 mmol/L EDTA, followed by fixation with BD Cytofix for 30 minutes on ice. Following a final wash, the cells were stored at 4°C until data acquisition using a LSRII using FACSDiva software (BD Biosciences). Analysis was performed using FlowJo software program (Tree Star Inc).

Animal studies

All the animal studies were performed in accordance with the ARRIVE guidelines and the 3 Rs rule of Replacement, Reduction and Refinement principles.

Mice were housed and treated following the protocols approved by the Institutional Animal Care and Use Committee at the University of California, San Francisco (San Francisco, CA)

and by the CEEA (Ethical Committee for the Use of Experimental Animals) at the Vall d'Hebron Institute of Oncology, Barcelona, Spain. Mouse weights were recorded for every experiment (Supplementary Fig. S1).

LSLKRas^{G12D};*Pdx1-cre* [Krastm4Tyj; Tg(Ipf1-cre)1Tuv] and *p53*$^{ER/ER}$ [Trp53tm1Gev] mice have been previously described (12–14). For all experiments, 8-week-old male and female *p53*$^{ER/ER}$;*LSLKRas*^{G12D};*Pdx1-cre* mice of mixed C57BL/6-FVB/N background were randomized into two groups: treated and control. Ibrutinib (0.16 mg/mL with 1% 2-Hydroxypropyl-beta-cyclodextrin; HP-β-CD) was added to the drinking water of treated animals, and control animals received water containing vehicle only (1% HP-β-CD). Vehicle or ibrutinib dissolved in water were both consumed at approximately 5.5 mL per day, in accordance with the reported typical daily water intake (15). Gemcitabine (75 mg/kg) was injected intraperitoneally twice a week for 3 weeks followed by a 1-week rest period. Sodium cromoglycate (10 mg/kg) was dissolved in saline solution and injected intraperitoneally, and control mice were treated with vehicle only. Endpoint criteria were defined as 20% body weight loss in addition to general morbidity and lethargy caused by tumor burden. Mice euthanized due to intestinal metaplasia or mucocutaneous papillomas caused by extrapancreatic KRAS^{G12D} expression were excluded from the survival study.

NOD/SCID mice were purchased from Charles River Laboratory. The anonymized human sample used was part of the tissue biologic material of the University Hospital Vall d'Hebron. The sample had been collected with a signed patient consent form and its use had been approved by the Ethics Committee (CEI) of the Hospital. The sample was randomly selected among the patient samples available. Heterotopic xenografts were generated from a tumor biopsy of a patient that underwent pancreatectomy at University Hospital Vall d'Hebron: when routine pathologic gross examination of a resected pancreas led to the detection of an adenocarcinoma, a slice with a thickness of 1 to 2 mm was transferred to RPMI-1640 media containing Antibiotic-Antimycotic (Gibco) and kept on ice; within approximately 30 minutes, the tissue sample was cut into pieces of 15 mm^3 under sterile conditions, suspended in Matrigel (BD Biosciences), and transported to the SPF area of the animal facility. A tumor piece was implanted subcutaneously into the flank of 2 to 3 female 6-week-old NOD/SCID mice. When successfully grafted tumors reached a size of about 750 mm^3, they were transplanted. The xenograft used for the study described here was transplanted to 6-week-old NOD/SCID females in generation 4, which after 6 weeks had produced a cohort of 28 mice with tumors measurable by caliper. Animals were randomized into two groups, 1 treated with ibrutinib and the other untreated. Tumor size was evaluated weekly by caliper measurements and tumor volume calculated using the following formula:

$$\text{volume} = \frac{\text{length} \times \text{width}^2}{2}$$

When tumor volume reached 1,500 mm^3, animals were euthanized and the tumor was collected and fixed overnight in neutral pH–buffered formalin.

Statistical analysis

Statistical analysis was carried out by two-tailed Mann–Whitney test (for IHC counts), two-tailed unpaired *t* test (for flow-cytometric data), χ^2 test of homogeneity (for collagen staining), and log-rank test (for Kaplan–Meier survival curves). SE (±SEM) and SD (±SD) are either represented in the graphs or following the means of all measures, as stated in figure legends. Statistical analysis was performed using GraphPad Prism 6.

Results

Ibrutinib strongly affects the tumor microenvironment in PDAC

We made use of a *p53*$^{ER/ER}$;*LSLKRas*^{G12D};*Pdx1-cre* mouse model that harbors a *Cre*-activated *KRas*^{G12D} allele inserted into the endogenous *KRas* locus, combined with pancreas-specific *Pdx1*-driven Cre recombinase activity (12, 16). The disruption of p53 signaling in combination with KRAS mutation leads to rapid tumorigenesis and histopathological features typical of human pancreatic adenocarcinoma within 8 weeks. At this stage, we treated the animals with ibrutinib, added at a dose of 35 mg/kg/d to their drinking water, or with vehicle control. No detectable side effects of the treatment were observed and the animals did not lose weight throughout (Supplementary Fig. S1). The animals were euthanized 4 weeks later and their pancreata harvested for analysis. As expected, mast cells were still recruited to the tumor stroma, but their degranulation was efficiently inhibited by ibrutinib treatment (Supplementary Fig. S2A). Strikingly, tumors treated with ibrutinib displayed a significant reduction in proliferation rate (Fig. 1A; 67.8 ± 29.5% Ki-67 positive in untreated vs. 14.9 ± 7.0% treated animals). CD11b-positive cells, as well as F4/80-positive macrophages were both reduced as shown by IHC and FACS analysis (Fig. 1B and C). However, the most striking change induced by ibrutinib treatment was on tumor fibrosis, reflected by collagen deposition as detected by Picrosirius Red staining. Treatment with ibrutinib dramatically reduced the amount of collagen present in the tumors (Fig. 1D and E).

The antifibrotic effect of ibrutinib is mast cell dependent

To verify that this effect on fibrosis was specifically due to mast cell interference, we first asked whether ibrutinib could have any direct activity on tumor cells *per se*. To address this question, we made use of four different pancreatic cancer cell lines and treated them with increasing amounts of ibrutinib *in vitro*, following their number over time. We chose four cell lines presenting a similar mutational profile to the one displayed by our mouse model (i.e., KRAS and p53 mutation): MIA PaCa-2, YAPC, PSN-1, and PA-TU-8988T. Importantly, none responded significantly to the treatment, pointing to the activity of ibrutinib on tumor stroma—rather than a direct effect on pancreatic cell survival—as the best candidate for ibrutinib's anti-tumorigenic effect in PDAC (Supplementary Fig. S3).

With this line of reasoning in mind and to verify the hypothesis that mast cell interference played a role in the antifibrotic effect displayed by ibrutinib, we performed two independent control experiments. In the first one, we made use of sodium cromoglycate (cromolyn), a well-characterized blocker of mast cell degranulation and inflammogen release (7, 17). We treated the *p53*$^{ER/ER}$; *LSLKRas*^{G12D};*Pdx1-cre* mice intraperitoneally (i.p.) with a daily

injection of 10 mg per kg (bodyweight) of cromolyn, starting at 8 weeks of age. The animals were euthanized 4 weeks later and their pancreata analyzed. We verified that cromolyn treatment blocked degranulation (Supplementary Fig. S2B). Strikingly, treatment with cromolyn recapitulated the antifibrotic effect displayed by ibrutinib (Fig. 2A and B). Once again, this effect was accompanied by a reduction in F4/80^{+} cells and a significant decrease in CD11b^{+} cells in the tumor stroma (Fig. 2C and D). Although cromolyn was also described to display some cytotoxic effect on pancreatic cancer cells (18), the overlapping effect of ibrutinib and cromolyn on collagen deposition strongly suggests that mast cell inhibition is the most likely explanation for this phenomenon. This finding is consistent with the recently published work showing that mast cells could exacerbate the cellular and extracellular dynamics of the tumor microenvironment found in PDAC (19).

In a second set of experiments, we made use of subcutaneous patient-derived xenografts (PDX) of a patient-derived tumor in NOD/SCID mice (Fig. 3). These mice are defective for both B- and T-cell function. Once again, ibrutinib prevented mast cell degranulation (Supplementary Fig. S2C) and led to a striking reduction in tissue fibrosis detected by Picrosirius Red staining (Fig. 3A and B), excluding B- and T-cell signaling modulation as ibrutinib's main mechanism of action in this context. The animals also showed a significant survival advantage when treated with ibrutinib compared with untreated littermates (Fig. 3C). Interestingly, IHC analysis of F4/80 and CD11b-positive cells showed a slight but nonsignificant reduction of both cell types (Fig. 3D and E).

These experimental models combined point to mast cells as crucial players in stimulating collagen deposition, in line with previously published data showing that mast cell tryptase might sustain liver fibrosis by promoting stellate cell proliferation and collagen synthesis (20) and with the concept that mast cells could be the culprit in various fibrotic diseases (21, 22).

Ibrutinib is an effective therapy and improves the outcome of standard care in a transgenic mouse model of PDAC

In PDAC, dense stromal fibrosis is a considerable obstacle to therapeutic intervention. Consequently, we hypothesized that the antifibrotic effect of ibrutinib represented a promising therapeutic opportunity. We therefore performed two independent survival experiments in the *p53*$^{ER/ER}$;*LSLKRas*^{G12D};*Pdx1-cre* mouse model: the first one sought to explore the therapeutic impact of ibrutinib alone and the second one to assess ibrutinib in combination with gemcitabine, the best characterized therapy available to pancreatic cancer patients during the past decade. As monotherapy, ibrutinib conferred a significant survival advantage to treated mice compared with untreated controls (Fig. 4A). In the second experiment, gemcitabine alone resulted in slight toxicity, although ibrutinib ameliorated the toxicity and significantly extended survival compared with gemcitabine alone (Fig. 4B), confirming our hypothesis that the standard-of-care outcome can be improved by the addition of ibrutinib.

Discussion

Our work provides preclinical evidence for the use of ibrutinib, which is already approved for clinical use, in the treatment of PDAC, based on the observed systemic mast cell inhibitory effects of ibrutinib as a potentially new and potent antifibrotic drug. In line with our results, it has been shown that ibrutinib specifically inhibits the release of IL8, MPC-1, and TNFα from mast cells (10). All these factors have a known role in fibrosis: IL8 is elevated in the serum of idiopathic pulmonary fibrosis patients (23) and correlates with the degree of fibrosis in infants with chronic liver disease (24); MCP-1 is a key determinant in the development of skin fibrosis, it could influence collagen fiber formation in mice (25) and is involved in the development of interstitial fibrosis in a mouse model of crescentic nephritis (26); finally, TNFα, which has a controversial role in fibrotic disease (27), promotes survival of activated hepatic stellate cells *in vitro* and *in vivo*, increases liver fibrosis in mice (28), mediates the transition from pulmonary inflammation to fibrosis (29) and its inhibition reduces fibrosis in a mouse model of autoimmune thyroiditis (30). Therefore, in addition to its beneficial role in reducing tumor fibrosis, the use of ibrutinib could potentially be extended to the treatment of various fibrotic diseases, such as liver fibrosis (31) or chronic pancreatitis (32).

The decrease in the leukocytic component of the tumor micro-environment (CD11b-positive cells and F4/80-positive macrophages) after treatment with ibrutinib and cromolyn could be explained by the fact that several chemokines produced by mast cells, such as IL6, are known to be potent stimulants for monocytic cell migration and macrophage activation (33), so that inhibiting mast cells could prevent their recruitment.

Intriguingly, recent work suggests that ibrutinib could be redeployed to treat lung cancer owing to inhibitory activity against the EGFR (34). However, EGFR mutations are not frequent in PDAC and none of our experimental systems presented EGFR alterations (data not shown).

It remains possible that additional anti-inflammatory effects of ibrutinib (specifically inhibition of B-cell signaling) might contribute to its therapeutic impact and modulation of other inflammatory components, even though we have demonstrated that such signaling is not required for decreased fibrosis. Further study of the effect of ibrutinib on other members of the complex PDAC stroma will be required to fully characterize its precise mechanism of action.

Supplementary Material

Refer to Web version on PubMed Central for supplementary material.

Acknowledgments

The authors thank Lisa Coussens for her valuable feedback and for useful reagents. The authors also acknowledge Dr. Joaquín Balsells and Dr. Maria Salcedo for their help in the collection and analysis of the patient derived tumor samples.

Grant Support

This work was supported by grants from the Miguel Servet Program (L. Soucek), the FERO Foundation (L. Soucek and D. Massó-Vallés), the Bear Necessities Pediatric Cancer Foundation (L. Soucek), Secretaria d'Universitats i Recerca del Departament déconomia i Coneixement de la Generalitat de Catalunya (D. Massó-Vallés), the European Social Fund (D. Massó-Vallés), and Asociación Española Contra el Cáncer (J. Arribas).

The costs of publication of this article were defrayed in part by the payment of page charges. This article must therefore be hereby marked *advertisement* in accordance with 18 U.S.C. Section 1734 solely to indicate this fact.

References

1. Hariharan D, Saied A, Kocher HM. Analysis of mortality rates for pancreatic cancer across the world. HPB. 2008; 10:58–62. [PubMed: 18695761]
2. Malvezzi M, Bertuccio P, Levi F, La Vecchia C, Negri E. European cancer mortality predictions for the year 2013. Ann Oncol. 2013; 24:792–800. [PubMed: 23402763]
3. Mahadevan D, Von Hoff DD. Tumor-stroma interactions in pancreatic ductal adenocarcinoma. Mol Cancer Ther. 2007; 6:1186–97. [PubMed: 17406031]
4. Koong AC, Mehta VK, Le QT, Fisher GA, Terris DJ, Brown JM, et al. Pancreatic tumors show high levels of hypoxia. Int J Radiat Oncol Biol Phys. 2000; 48:919–22. [PubMed: 11072146]
5. Strouch MJ, Cheon EC, Salabat MR, Krantz SB, Gounaris E, Melstrom LG, et al. Crosstalk between mast cells and pancreatic cancer cells contributes to pancreatic tumor progression. Clin Cancer Res. 2010; 16:2257–65. [PubMed: 20371681]
6. Cai SW, Yang SZ, Gao J, Pan K, Chen JY, Wang YL, et al. Prognostic significance of mast cell count following curative resection for pancreatic ductal adenocarcinoma. Surgery. 2011; 149:576–84. [PubMed: 21167541]
7. Soucek L, Lawlor ER, Soto D, Shchors K, Swigart LB, Evan GI. Mast cells are required for angiogenesis and macroscopic expansion of Myc-induced pancreatic islet tumors. Nat Med. 2007; 13:1211–8. [PubMed: 17906636]
8. Chang DZ, Ma Y, Ji B, Wang H, Deng D, Liu Y, et al. Mast cells in tumor microenvironment promotes the *in vivo* growth of pancreatic ductal adenocarcinoma. Clin Cancer Res. 2011; 17:7015–23. [PubMed: 21976550]
9. Byrd JC, Furman RR, Coutre SE, Flinn IW, Burger JA, Blum KA, et al. Targeting BTK with ibrutinib in relapsed chronic lymphocytic leukemia. N Engl J Med. 2013; 369:32–42. [PubMed: 23782158]
10. Chang BY, Huang MM, Francesco M, Chen J, Sokolove J, Magadala P, et al. The Bruton tyrosine kinase inhibitor PCI-32765 ameliorates autoimmune arthritis by inhibition of multiple effector cells. Arthritis Res Ther. 2011; 13:R115. [PubMed: 21752263]
11. Soucek L, Buggy JJ, Kortlever R, Adimoolam S, Monclus HA, Allende MT, et al. Modeling pharmacological inhibition of mast cell degranulation as a therapy for insulinoma. Neoplasia. 2011; 13:1093–100. [PubMed: 22131884]
12. Christophorou MA, Martin-Zanca D, Soucek L, Lawlor ER, Brown-Swigart L, Verschuren EW, et al. Temporal dissection of p53 function *in vitro* and *in vivo*. Nat Genet. 2005; 37:718–26. [PubMed: 15924142]
13. Hingorani SR, Petricoin EF, Maitra A, Rajapakse V, King C, Jacobetz MA, et al. Preinvasive and invasive ductal pancreatic cancer and its early detection in the mouse. Cancer Cell. 2003; 4:437–50. [PubMed: 14706336]
14. Jackson EL, Willis N, Mercer K, Bronson RT, Crowley D, Montoya R, et al. Analysis of lung tumor initiation and progression using conditional expression of oncogenic K-ras. Genes Dev. 2001; 15:3243–8. [PubMed: 11751630]
15. Bachmanov AA, Reed DR, Beauchamp GK, Tordoff MG. Food intake, water intake, and drinking spout side preference of 28 mouse strains. Behav Genet. 2002; 32:435–43. [PubMed: 12467341]
16. Hingorani SR, Wang L, Multani AS, Combs C, Deramaudt TB, Hruban RH, et al. Trp53R172H and KrasG12D cooperate to promote chromosomal instability and widely metastatic pancreatic ductal adenocarcinoma in mice. Cancer Cell. 2005; 7:469–83. [PubMed: 15894267]
17. Thompson PJ, Hanson JM, Morley J. Asthma, mast cells, and sodium cromoglycate. Lancet. 1983; 2:848–9.

18. Arumugam T, Ramachandran V, Logsdon CD. Effect of cromolyn on S100P interactions with RAGE and pancreatic cancer growth and invasion in mouse models. J Natl Cancer Inst. 2006; 98:1806–18. [PubMed: 17179482]
19. Ma Y, Hwang RF, Logsdon CD, Ullrich SE. Dynamic mast cell-stromal cell interactions promote growth of pancreatic cancer. Cancer Res. 2013; 73:3927–37. [PubMed: 23633481]
20. Gaca MD, Zhou X, Benyon RC. Regulation of hepatic stellate cell proliferation and collagen synthesis by proteinase-activated receptors. J Hepatol. 2002; 36:362–9. [PubMed: 11867180]
21. Hugle T. Beyond allergy: the role of mast cells in fibrosis. Swiss Med Wkly. 2014; 144:w13999. [PubMed: 25184789]
22. Overed-Sayer C, Rapley L, Mustelin T, Clarke DL. Are mast cells instrumental for fibrotic diseases? Front Pharmacol. 2013; 4:174. [PubMed: 24478701]
23. Ziegenhagen MW, Zabel P, Zissel G, Schlaak M, Muller-Quernheim J. Serum level of interleukin 8 is elevated in idiopathic pulmonary fibrosis and indicates disease activity. Am J Respir Crit Care Med. 1998; 157:762–8. [PubMed: 9517588]
24. Nobili V, Marcellini M, Giovannelli L, Girolami E, Muratori F, Giannone G, et al. Association of serum interleukin-8 levels with the degree of fibrosis in infants with chronic liver disease. J Pediatr Gastroenterol Nutr. 2004; 39:540–4. [PubMed: 15572896]
25. Ferreira AM, Takagawa S, Fresco R, Zhu X, Varga J, DiPietro LA. Diminished induction of skin fibrosis in mice with MCP-1 deficiency. J Invest Dermatol. 2006; 126:1900–8. [PubMed: 16691201]
26. Lloyd CM, Dorf ME, Proudfoot A, Salant DJ, Gutierrez-Ramos JC. Role of MCP-1 and RANTES in inflammation and progression to fibrosis during murine crescentic nephritis. J Leukoc Biol. 1997; 62:676–80. [PubMed: 9365123]
27. Distler JH, Schett G, Gay S, Distler O. The controversial role of tumor necrosis factor alpha in fibrotic diseases. Arthritis Rheum. 2008; 58:2228–35. [PubMed: 18668576]
28. Pradere JP, Kluwe J, De Minicis S, Jiao JJ, Gwak GY, Dapito DH, et al. Hepatic macrophages but not dendritic cells contribute to liver fibrosis by promoting the survival of activated hepatic stellate cells in mice. Hepatology. 2013; 58:1461–73. [PubMed: 23553591]
29. Oikonomou N, Harokopos V, Zalevsky J, Valavanis C, Kotanidou A, Szymkowski DE, et al. Soluble TNF mediates the transition from pulmonary inflammation to fibrosis. PLoS ONE. 2006; 1:e108. [PubMed: 17205112]
30. Chen K, Wei Y, Sharp GC, Braley-Mullen H. Decreasing TNF-alpha results in less fibrosis and earlier resolution of granulomatous experimental autoimmune thyroiditis. J Leukoc Biol. 2007; 81:306–14. [PubMed: 17046971]
31. Bataller R, Brenner DA. Liver fibrosis. J Clin Invest. 2005; 115:209–18. [PubMed: 15690074]
32. Homma T, Harada H, Koizumi M. Diagnostic criteria for chronic pancreatitis by the Japan Pancreas Society. Pancreas. 1997; 15:14–5. [PubMed: 9211487]
33. Clahsen T, Schaper F. Interleukin-6 acts in the fashion of a classical chemokine on monocytic cells by inducing integrin activation, cell adhesion, actin polymerization, chemotaxis, and transmigration. J Leukoc Biol. 2008; 84:1521–9. [PubMed: 18765478]
34. Gao W, Wang M, Wang L, Lu H, Wu S, Dai B, et al. Selective antitumor activity of ibrutinib in EGFR-mutant non-small cell lung cancer cells. J Natl Cancer Inst. 2014; 106

Europe PMC Funders Author Manuscripts

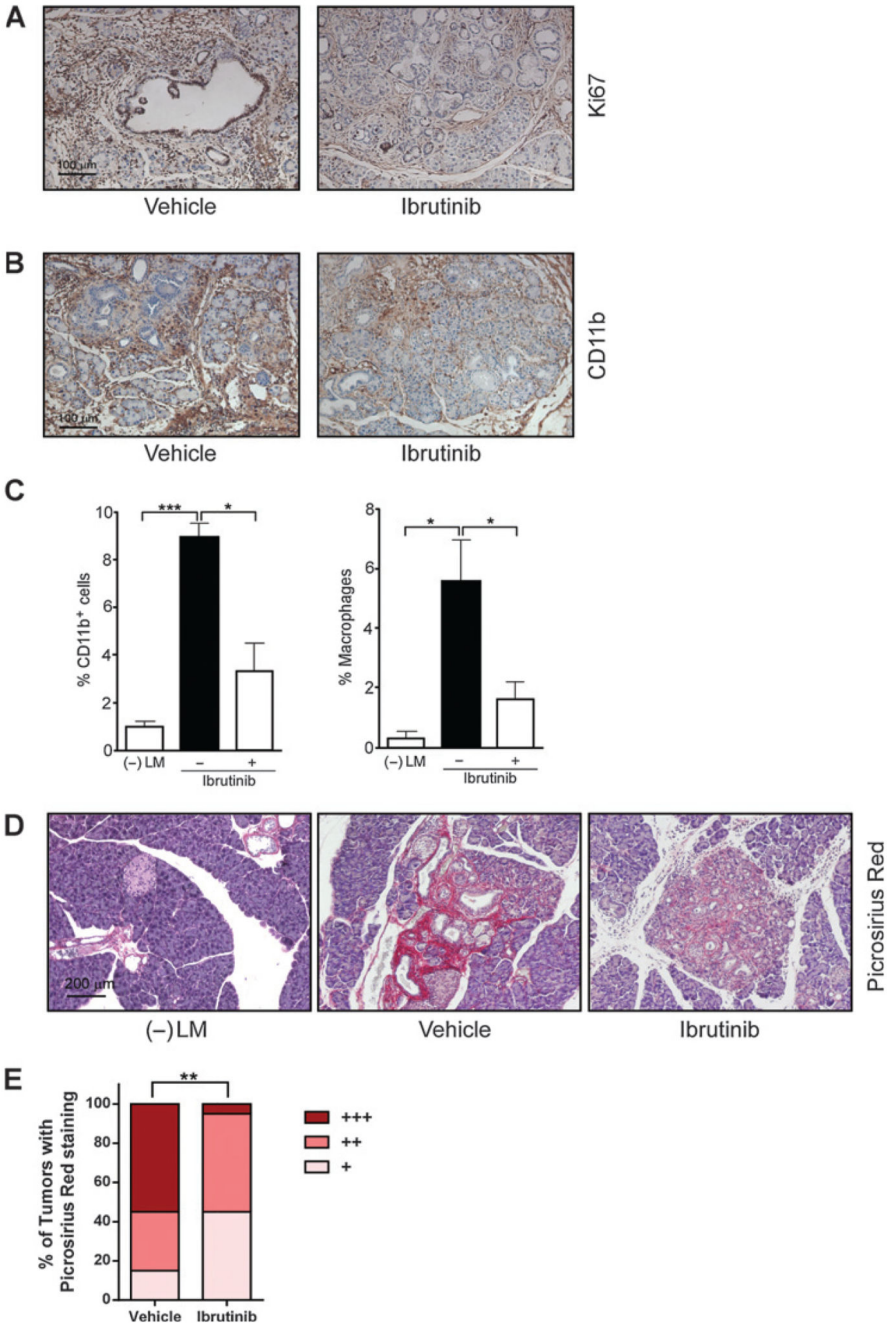

Figure 1. Ibrutinib treatment has a profound effect on the tumor microenvironment.

A, 8-week-old *p53*$^{ER/ER}$;*LSLKRas*^{G12D};*Pdx1-cre* mice were treated with ibrutinib (n = 4) or vehicle control (n = 4) for 4 weeks. Histologic analysis of pancreata shows a reduction in Ki-67–positive (proliferating) cells in ibrutinib-treated mice (mean ± SD = 14.9 ± 7.0%) compared with control animals (67.8 ± 29.5%; P = 0.0016, two-tailed Mann–Whitney test). Three animals per condition and five sections per animal were analyzed. All cells in the tumor area were scored, independently of their cell type. B, IHC for CD11b (a leukocytic marker associated with monocytes, neutrophils, natural killer cells, granulocytes, and

Europe PMC Funders Author Manuscripts

macrophages) shows a clear reduction of CD11b positivity in ibrutinib-treated compared with vehicle-treated mice. C, percentages of $CD11b^+$ cells ($CD45^+CD11c^-$) and tumor-associated macrophages ($CD45^+CD11b^+Ly6C^-Ly6G^-F4/80^+$) in single cell suspensions of normal pancreas isolated from negative untreated littermates [(–)LM], and from tumor-bearing mice treated with ibrutinib or vehicle, as assessed by flow cytometry and expressed as a percentage of total cells. Results shown represent mean ± SEM. Statistical significance was determined via unpaired *t* test with *, $P < 0.05$; **, $P < 0.01$; ***, $P < 0.001$. At least three animals per condition were analyzed. D, Picrosirius Red staining of pancreatic samples from negative littermates [(–)LM] and from tumor-bearing mice treated with ibrutinib or vehicle. Animals treated with ibrutinib show a reduced amount of collagen compared with vehicle-treated animals. Four animals per condition and five sections per animal were analyzed. Red staining shows collagen in the tumor stroma. E, scoring of treated ($n = 20$) and untreated ($n = 20$) tumors according to their collagen content shows a significant difference between groups ($P = 0.0021$). Sections stained with Picrosirius Red staining were scored blindly and assigned to three categories (+, ++, or +++). The percentages of tumors classified into each category are shown. A χ^2 test of homogeneity was utilized for statistical analysis of the data.

Europe PMC Funders Author Manuscripts

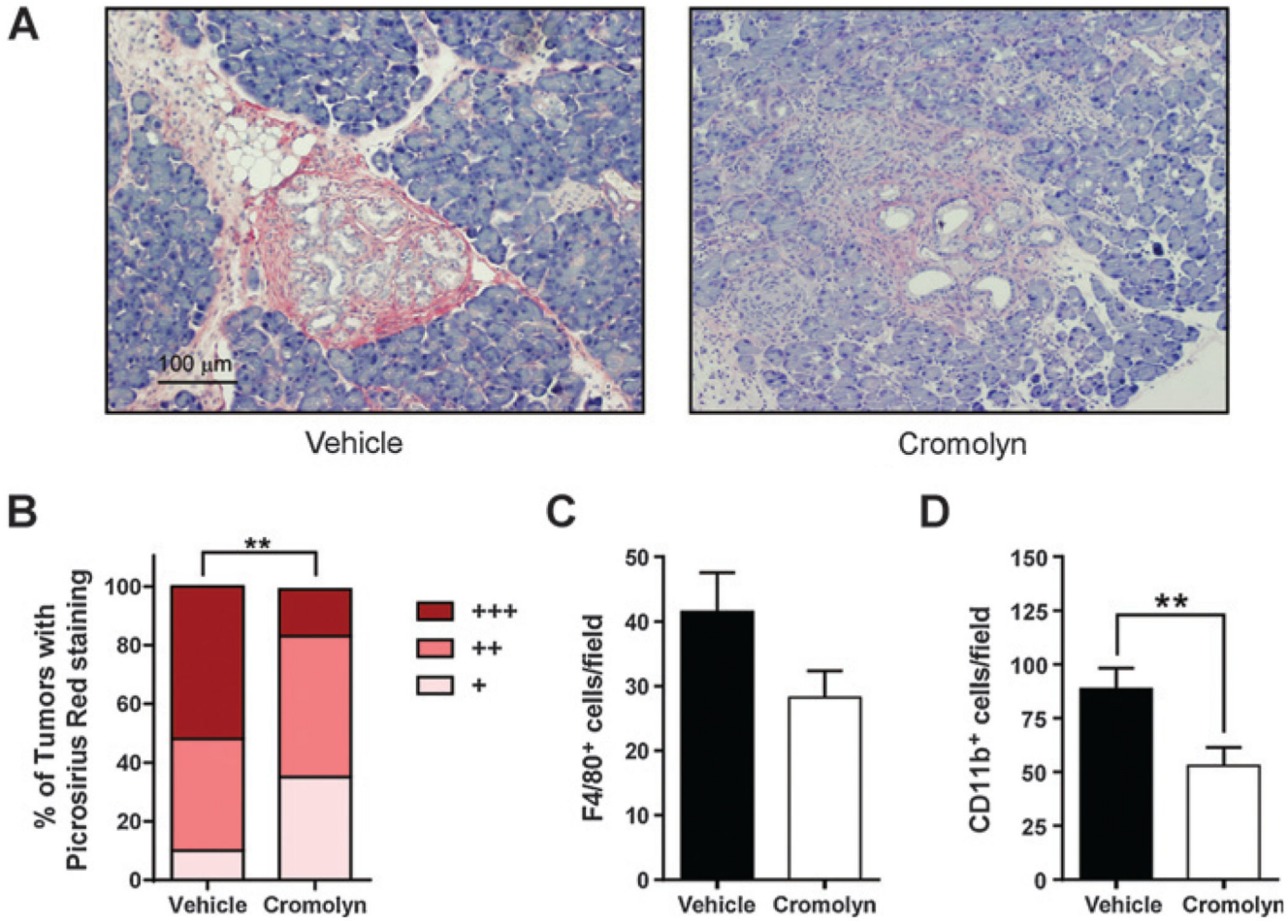

Figure 2. Mast cell function inhibition by cromolyn diminishes tissue fibrosis.

A, 8-week-old *p53*$^{ER/ER}$;*LSLKRas*^{G12D};*Pdx1-cre* mice were treated with intraperitoneal sodium cromoglycate ($n = 6$) or vehicle control ($n = 5$) for 4 weeks. Histologic analysis of pancreata by Picrosirius Red staining shows reduced collagen deposition in cromolyn-treated mice compared with vehicle-treated control animals. Five animals per condition and at least five sections per animal were analyzed. Red staining shows collagen in the tumor stroma. B, scoring of treated ($n = 30$) and untreated ($n = 25$) tumors according to their collagen content shows a significant difference between groups (**, $P = 0.0083$). Sections stained with Picrosirius Red staining were scored blindly and assigned to three categories (+, ++, or +++). The percentages of tumors classified into each category are shown. A χ^2 test of homogeneity was utilized for statistical analysis of the data. C, quantification of F4/80-positive cells per microscopic field in the tumor area shows a nonsignificant reduction in cromolyn-treated versus vehicle-treated mice. Results shown represent mean ± SEM. Five animals per condition and four sections per animal were analyzed. Statistical significance was determined via two-tailed Mann–Whitney test. D, quantification of CD11b-positive cells per microscopic field in the tumor area shows a significant reduction in cromolyn-treated versus vehicle-treated mice (**, $P = 0.0021$, two-tailed Mann–Whitney test). Results

shown represent mean ± SEM. Five animals per condition and four sections per animal were analyzed.

Europe PMC Funders Author Manuscripts

Europe PMC Funders Author Manuscripts

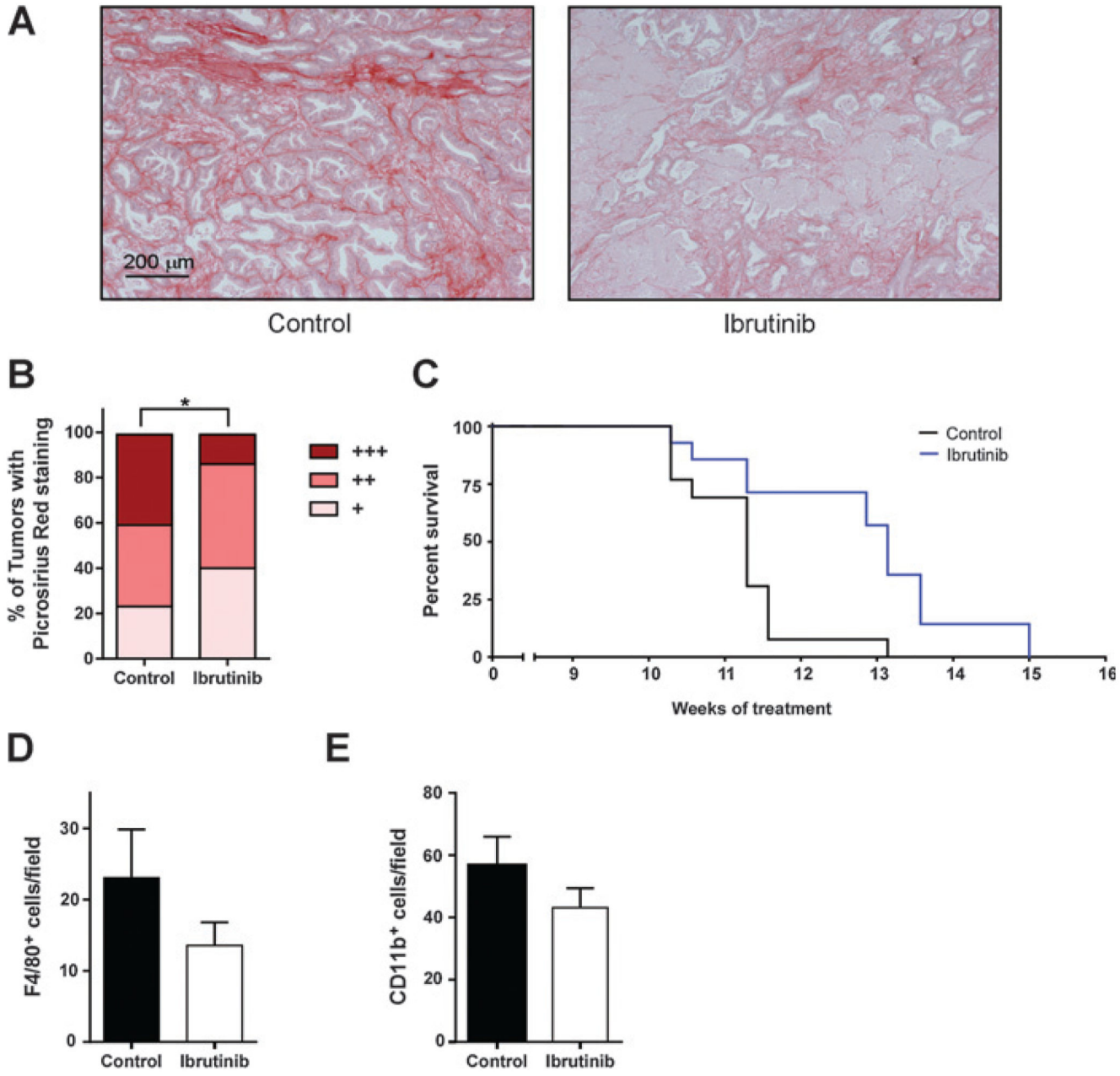

Figure 3. Ibrutinib treatment diminishes tissue fibrosis in a PDX model of PDAC.

A, ibrutinib treatment reduces collagen deposition in subcutaneous xenografts of a patient-derived tumor in NOD/SCID mice. Picrosirius Red staining was performed on tumor samples from untreated ($n = 6$) or ibrutinib-treated mice ($n = 6$) and indicates collagen deposition in the tumor stroma. Six animals per condition and four sections per animal were analyzed. B, scoring of sections from treated ($n = 26$) and untreated ($n = 26$) tumors according to their collagen content shows a significant difference between groups (*, $P = 0.039$). Sections stained with Picrosirius Red were scored blindly and assigned to three categories (+, ++, or +++). The percentages of tumors classified into each category are shown. A χ^2 test of homogeneity was utilized for statistical analysis of the data. C, NOD/

SCID mice subcutaneously transplanted with a patient-derived tumor were treated with ibrutinib ($n = 14$) or untreated ($n = 13$) starting from 8 weeks of age. Ibrutinib alone confers survival advantage to the treated animals ($P = 0.0021$, log-rank test). D, quantification of F4/80-positive cells per microscopic field on the border of the subcutaneous tumors shows a nonsignificant reduction in ibrutinib-treated versus control mice. Results shown represent mean ± SEM. At least three animals per condition and four sections per animal were analyzed. Statistical significance was determined via two-tailed Mann–Whitney test. E, quantification of CD11b-positive cells per microscopic field on the border of the subcutaneous tumors shows a nonsignificant reduction in ibrutinib-treated versus control mice. Results shown represent mean ± SEM. At least three animals per condition and four sections per animal were analyzed. Statistical significance was determined via two-tailed Mann–Whitney test.

Europe PMC Funders Author Manuscripts

Europe PMC Funders Author Manuscripts

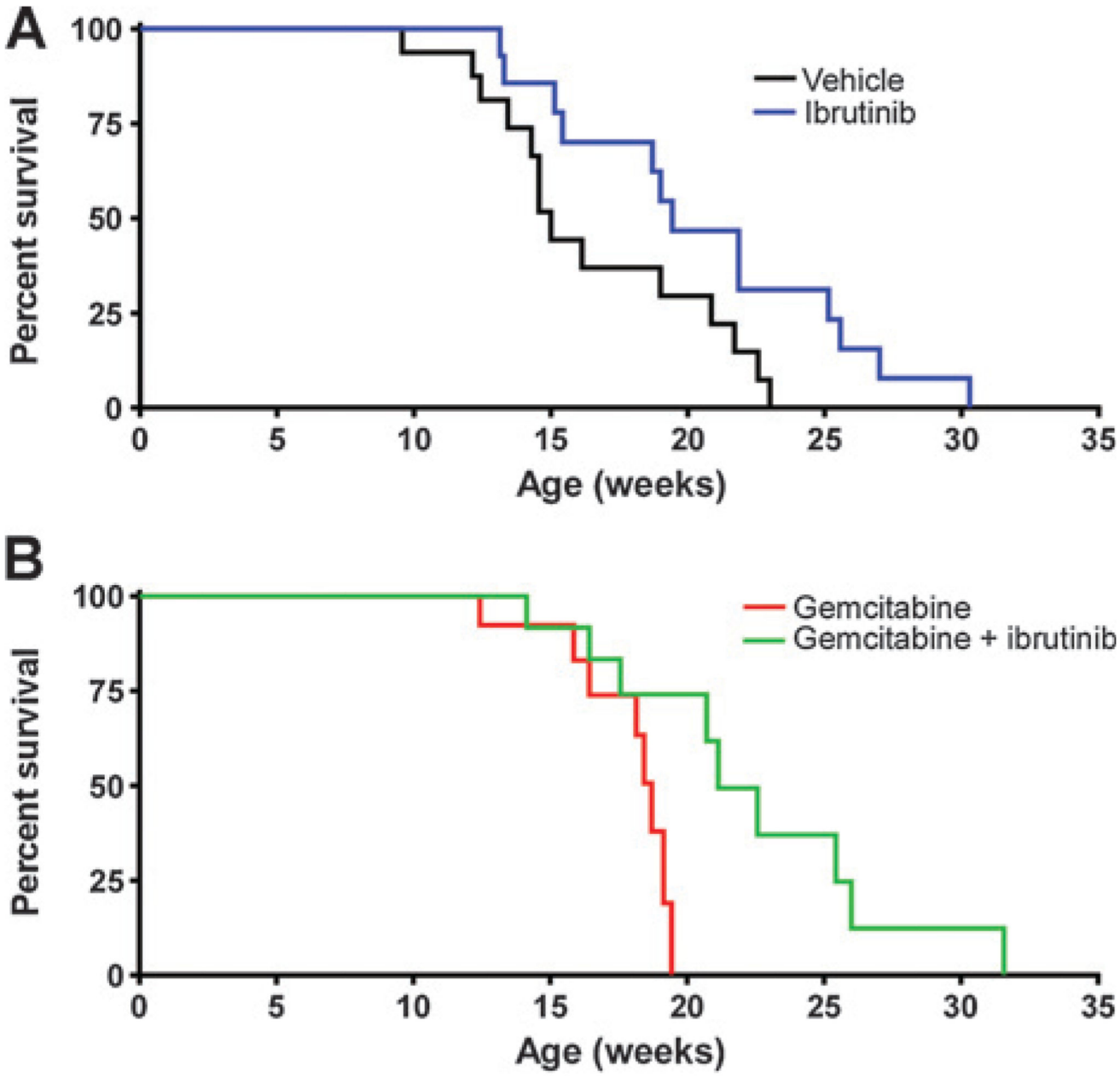

Figure 4. Ibrutinib has a significant therapeutic impact as monotherapy and in combination with standard of care. Two independent experiments were conducted to determine the survival effect of ibrutinib.

A, *p53*$^{ER/ER}$;*LSLKRas*^{G12D};*Pdx1-cre* mice were treated with ibrutinib (n = 14) or vehicle control (n = 13) starting from 8 weeks of age. Ibrutinib alone confers survival advantage to the treated animals (P = 0.030, log-rank test). B, *p53*$^{ER/ER}$;*LSLKRas*^{G12D};*Pdx1-cre* mice were treated with gemcitabine (n = 8) or with a combination of gemcitabine and ibrutinib (n = 9), starting from 8 weeks of age. The addition of ibrutinib to standard of care improves animal survival (P = 0.025, log-rank test).